24th COBEM - 2017

24th ABCM International Congress of Mechanical Engineering
December 3-8, 2017, Curitiba, PR, Brazil

COBEM-2017-1231
MATHEMATICAL MODEL FOR THE THERMAL-HYDRAULIC CALCULATION IN A FRESNEL LINEAR REFLECTOR SYSTEM

Ewerton Felipe de Souza Cordeiro
Gabriel Ivan Medina Tapia
Universidade Federal do Rio Grande do Norte, Campus Universitário, Departamento de Engenharia Mecânica, Laboratório de Sistemas Térmicos e Energias Alternativas – LSTEA, Lagoa Nova, CEP 59072-970, Natal/RN, Brasil
ewertonfelipec@gmail.com, gmedinat@ct.ufrn.br

Abstract. *In the development of a Linear Fresnel Reflector (LFR) system, the calculation of temperature distribution, steam quality and pressure drop are very important. So, in this paper, was developed a mathematical model for the thermo-hydraulic calculations in steady-state on the LFR system, where the differential equations originated from of the thermal balance of the continuity equations, of the linear movement quantity and in the energy equation were solved simultaneously. The developed model allows the calculation of the variation of temperature of the working fluid, pressure drop troughout the system and the variation of the heat flux, for different conditons of direct normal irradiance(DNI). With the obtained results was possible to comprehend the behaivor of the fluid for different DNI conditions, as well as to simulate the thermal efficiency of the system and observe that this parameter is very important in the simulation of system.*

Keywords: *LFR, CSP, Thermo-hydraulic*

1. INTRODUCTION

Power generation systems with solar concentrators (CSP) have as its fundamental principle converting thermal energy into electric energy by means of an indirect process. Generally, this type of technology requires a relatively large area of mirrors to converge the solar radiation into a receiver, where there is a working fluid that is heated to high temperatures to be employed in a thermodynamic cycle directly or serving to exchange heat with another fluid that can participate in the cycle and generate electricity, according to Zhu (2013). There are four types of CSP technology: Stirling dish, parabolic trough, solar tower plant and Fresnel technology.

The LFR technology was chosen for this paper because is a promising technology that presents advantages over other CSP systems, such as low assembly and maintenance costs, low cost of structural supports and reflectors, and smaller occupied land areas by the solar concentration camps (Cau and Cocco, 2014). Another relevant characteristic of this system is that the power reception for power generation is the largest per unit of occupied area, which is a preponderant factor for countries that have low availability of land areas for installation of the power plants. Therefore, this technology is considered as a low-cost alternative for power generation through thermal processes (Silva Junior, 2015).

According to Sahoo et al (2012a), the LFR system consists on use of a series of long and flat mirrors that focus the sun's radiation on a fixed receiver formed by a set of SS304 stainless steel tubes, straight and parallel allotted in a cavity, generally trapezoidal, where the flow of energy is concentrated from the mirrors located just above the ground, as can be seen in Fig. 1. The interior of the cavity, external to the tubes, contains air that is not in contact with the environment due to the glass coverage at the bottom of the cavity. The working fluid flows through the tubes into the cavity and absorbs heat from the solar rays reflected by the surface of the LFR system. The working fluid enters the pipes at high pressure and increases its temperature until it reaches the saturation temperature due to the absorbed heat. Soon after achieving saturation, the steam quality increases as it reaches the two-phase region and is delivered to the thermodynamic cycle of power generation, usually a Rankine Cycle.

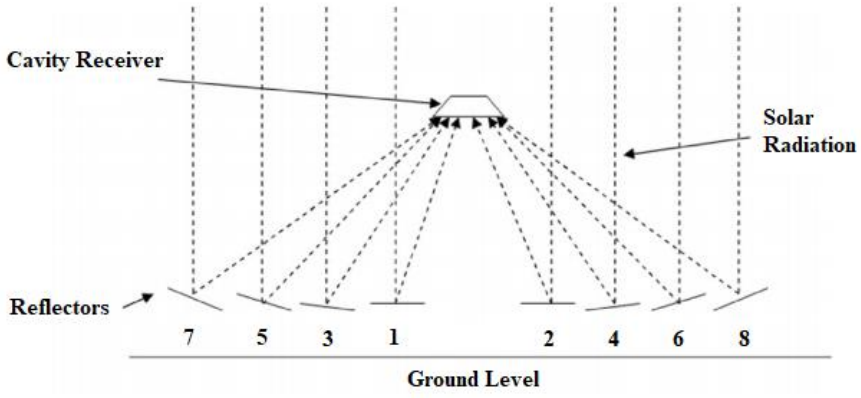

Figure 1. Representation of the LFR system. (Sahoo 2012b)

For the selection of the working fluid, it was taken into account that water is recommended for systems that will operate at temperatures up until *220 °C* and that thermal oils are ideal for systems operating at temperatures above *250 °C*. Therefore, it was defined that the water would enter the pipes at a pressure of *20 bar*, which leads to a saturation temperature of *212.4 °C* and as the analysis performed is not intended to be delivered to the power generation cycle superheated steam, this saturation temperature is the output temperature of the system. In addition to water and thermal oils and according to Morin et al. (2015), molten salt can be used as work fluid in LFR systems.

In the LFR system, each mirror has a slope, with an orientation system that follows the path from the sun to the west and reflects the solar radiation into the absorber, efficiently, throughout the period of sunlight availability. However, optical losses related to mirrors, such as shading, blocking and cosine effects, can be reduced increasing the spacing between the mirrors.

The two main applications for Fresnel technology are the large-scale production of electrical energy and the heat production process for the food, textile, chemical and metallurgical industries. The Figure 2 represents the Fresnel technology applied to the production of electric energy, showing all the operation of the LFR system from the entrance of the working fluid in the pipes, through the thermodynamic cycle of power generation until the generation of electricity.

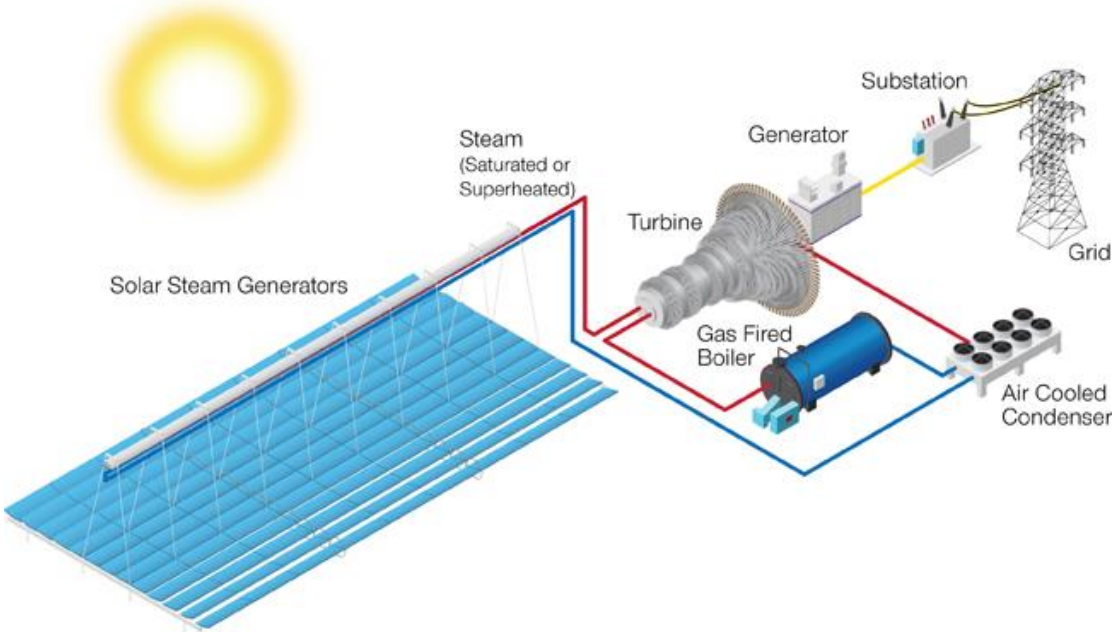

Figure 2. Schematic representation of an LFR system applied to electric power generation. (AREVA)

2. METODOLOGY

At first, it was necessary to obtain DNI data from the city of Natal / RN, taken from the INPE (Instituto Nacional de Pesquisas Espaciais), which through the LAVAT (Laboratório de Variáveis Ambientais Tropicais) makes measurements of solarmetric data with small intervals, which does not provide an exact value, but very close to the reality of the

conditions of the city. In the present study, a mean DNI was used, comprising a work range from 10h to 13h, differently from what normally occurs, because the DNI varies at each moment of the day. The parameters of the trapezoidal cavity, tubes and the angulation of each mirror were based on the Sahoo et al (2012a) and Silva Junior (2015), according Tab. 1.

Table 1. Geometrical parameters of tubes and mirrors.

DESCRIPTION	DIMENSIONS
Bottom width of cavity	500 mm
Top width of cavity	300 mm
Side width of cavity	141 mm
Depth of cavity	100 mm
Number of tubes	8
Inner diameter of absorber tube	26.7 mm
Outer diameter of absorber tube	33.4 mm
Absorber length	420 m
Number of reflector mirrors	8
Reflector width	1.8 m
Position of reflectors from ground	1 m
Position of absorber from ground	13 m
Angle of reflector mirrors 1 and 2	5°
Angle of reflector mirrors 3 and 4	15°
Angle of reflector mirrors 5 and 6	30°
Angle of reflector mirrors 7 and 8	45°

A balance of energy and moments of the system were performed in the tube, as shown Fig. 3, the following considerations have been taken into account to obtain the model:

- Consider that the absorber tube is long, straight and uninterrupted;
- The heat flux is constant along the tubes;
- Heat transfer is considered one-dimensional;
- The analysis is focused on the study of external fluid temperature;
- The steam outlet condition is dry or wet.

After the considerations have been made, the principles of conservation of mass, energy and momentum, were expressed by Eqs. (1), (2) and (3), respectively, in the form of differential equations, are observed in the tubes.

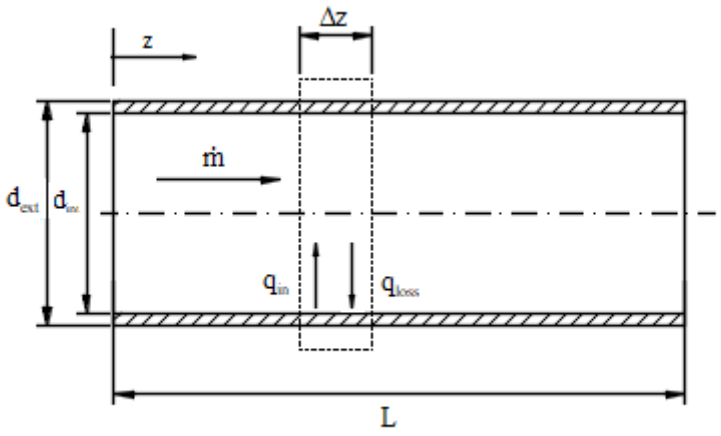

Figure 3. Schematic representation of the tubes located in the receiver.

$$\frac{d}{dz}(\rho v A) = 0 \tag{1}$$

$$\dot{m}\frac{de}{dz} = (q''_{in} - q''_{loss})S \tag{2}$$

$$-\frac{dP}{dz}=\frac{1}{A}\frac{d(\rho v^2 A)}{dz}+\tau_w\frac{S}{A} \tag{3}$$

Where ρ is the density of the fluid, v is the velocity that the fluid moves within the tubes and A is the cross-sectional area of the tube. The $\dot{m}$ is the mass flow that passes through the tubes, q''_{in} is the heat flow that enters on the receiver, whereas q''_{loss} is the heat loss flow and S the perimeter of tube. The τ_w is the shear stress acting on the inner tube. The de/dz means the variation of energy along the subdomain z and dP/dz the variation of pressure in the subdomain.

The Eqs. (2) e (3) were discretized by the finite difference method with progressive difference, which guarantees a small error range, according to Carnahan et al. (1969). The method of finite difference aims to transform a problem composed of differential equations into a problem formed by algebraic equations. Discretization consists of dividing the calculation domain into some subdomains (Carnahan et al, 1969). In the present paper, the calculation domain was divided into subdomains (z) of 1 meter in length, generating a uniform mesh. The discretized equations in the single-phase region are represented in Eqs. (4) and (5), and the discrete equations in the biphasic region are represented in Eqs. (6) and (7).

$$\frac{P_{z+1}-P_z}{dz}-\frac{1}{A}\left[\frac{(\rho_l v_l^2 A)_{z+1}-(\rho_l v_l^2 A)_z}{dz}\right]-\tau_w\frac{S}{A}=0 \tag{4}$$

$$\dot{m}\frac{\left[cp(T_{z+1}-T_z)+\left(\frac{v_{l,z+1}^2-v_{l,z}^2}{2}\right)\right]}{dz}-[q''_{in}-U(T_t-T_a)]S=0 \tag{5}$$

$$\frac{P_{z+1}-P_z}{dz}-\frac{1}{A}\left[\frac{(\rho_h v_h^2 A)_{z+1}-(\rho_h v_h^2 A)_z}{dz}\right]-\tau_w\frac{S}{A}=0 \tag{6}$$

$$\dot{m}\frac{1}{dz}\left[\left([h_l+x\cdot h_{lv}]_{z+1}-[h_l+x\cdot h_{lv}]_z\right)+\left(\frac{v_{h,z+1}^2-v_{h,z}^2}{2}\right)\right]-[q''_{in}-U(T_t-T_a)]S=0 \tag{7}$$

The subscript ($z + 1$) indicates that it is the value downstream of the last evaluated point, c_P is the specific heat at constant pressure, T is the temperature of the fluid, U is the overall coefficient of heat loss, T_t is the temperature of the outer wall of the tubes and T_a is the ambient temperature. The subscript l indicates that the property is in the liquid phase and the subscript lv indicates that it is in the liquid-vapor mixing region. The h is the enthalpy of the work fluid and the x indicates the title, that is, the steam quality.

The thermo-hydraulic analysis performed in this paper was divided into two parts, analyzing the heat loss in the cavity and the convective flow inside the tubes, as shown in Fig. 4. The heat transfer in the trapezoidal cavity involves the three types of heat transfer, but the radiation and convection types predominate. The heat loss by conduction through the insulated sides of the absorber being taken into account.

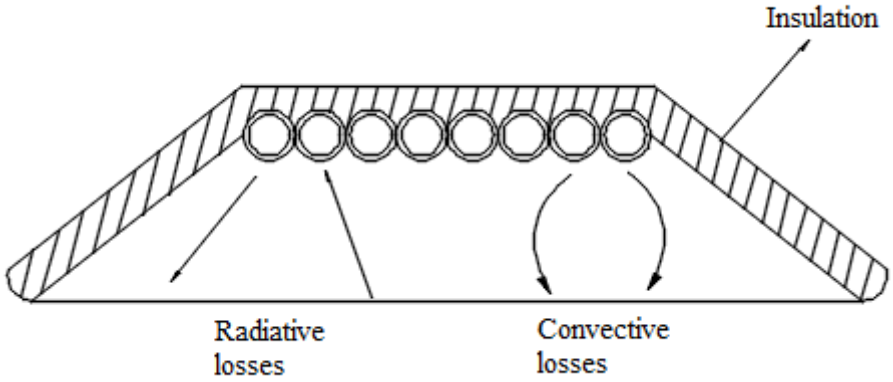

Figure 4. Representation of heat transfer in the trapezoidal cavity.

An average value of the overall heat loss coefficient of the absorber cavity was used according to results obtained by Singh et al (2010) by the cavity correlation estimation method. The method consists in calculate the losses coefficients of radiation and convection of the absorber through the glass coverage and calculate the loss coefficient by conduction of the insulated sides, where, the sum of these two values show the overall coefficient of heat loss. The correlations explained by Balaji and Venkatesan (1994) to estimate the Nusselt numbers for convection and radiation were obtained by the Grashof number using also the radiation-conduction interaction parameter and the temperature ratio. With these values, the coefficients of convective and radiative heat transfer between the absorber and the glass coverage and the coefficients of radiation and convection on the outer surface of the glass cover are calculated.

For the analysis of convective flow in the absorber, the fluid enters the tube with known and stable thermodynamic state. The tube is subjected to a uniform heat flow on its outer surface and to a variation of heat loss while the fluid remains in the single-phase region. After boiling, in the biphasic region, the liquid heat flux remains practically constant. The input heat flux is expressed by Eq. (8), this equation was developed by Sahoo et al. (2012b) specifically for the LFR system, taking into consideration the *DNI*, characteristic of the mirrors and characteristics of the tubes. The heat loss flow is shown in Eq. (9) which is the product of the overall heat loss coefficient with the temperature variation between the outer wall of the tube and the ambient temperature.

$$q''_{in} = \frac{DNI \cdot \rho_e \cdot (\sum A_{ref} \cdot \cos\theta) \cdot \gamma \cdot (\tau\alpha)}{n_t \cdot \pi \cdot d_{ext} \cdot L} \tag{8}$$

$$q''_{loss} = U(T_t - T_a) \tag{9}$$

In Eq. (8), the ρ_e is the reflectance of the reflecting mirrors, A_{ref} is the surface area of the reflectors that multiplied to the inclination angle of the reflectors provides the area being reflected to the trapezoidal receiver. The symbols γ and $\tau\alpha$ are properties of the reflecting mirrors, respectively, solidity and transmissivity-absorbance factor. The number of tubes is given in n_t, L is the length of the absorber tubes and d_{ext} is the outer diameter of the tubes.

Eqs. (10), (11) and (12) represent the specific mass, enthalpy and a dimensionless factor in the biphasic region, respectively. These equations were taken in Sahoo et al (2012a).

$$\rho_h = \rho_g \cdot \alpha + \rho_l(1-\alpha) \tag{10}$$

$$h_h = h_l + x \cdot h_{lv} \tag{11}$$

$$\alpha = \left(1 + \left(\frac{1-x}{x}\right)\frac{\rho_g}{\rho_l}\right)^{-1} \tag{12}$$

The subscript *h* means a homogeneous quantity, in the region of single phase this term can be treated as *l*. The subscript *g* represents gas and the α is a dimensionless factor for the biphasic region.

Along the tube, the fluid is always in contact with the pipe wall, causing a friction loss and consequently a shear stress, so to calculate this stress using Eq. (13) where the friction factor, *f*, for the single-phase region is estimated by the correlation of Swamee and Jain (1976) expressed in Eq. (14). In the biphasic region it is necessary to consider the phase multiplier in the shear stress, ϕ_{fr}^2. Therefore, Eqs. (15) and (16) represent the shear stress and the friction factor in the biphasic region, f_{lo}. The two-phase multiplier, expressed in Eq. (17), is given by Friedel's correlation, since, according to Pye (2008), this correlation generates better results when compared with other correlations. Eq. (18) expresses the temperature of the working fluid in terms of the outer wall of the tube, according to Sahoo et al. (2012a).

$$\tau_w = \frac{1}{2} f \frac{\dot{m}}{A^2 \cdot \rho_l} \tag{13}$$

$$f = \frac{0.25}{\left[\log_{10}\left(\frac{\varepsilon_d}{3.7 \cdot d_{int}} + \frac{5.74}{Re_D^{0.9}}\right)\right]^2} \tag{14}$$

$$\tau_w = \frac{1}{2} f_{lo} \frac{\dot{m}}{A^2 \cdot \rho_l} \phi_{fr}^2 \tag{15}$$

$$f_{lo} = \frac{0.079}{Re_D^{0.25}} \tag{16}$$

$$\phi_{fr}^2 = E + \frac{3.24 \cdot F \cdot H}{F_{rh}^{0.045} \cdot W_{el}^{0.035}} \tag{17}$$

$$(q''_{in} - q''_{loss})S = \frac{T_t - T}{\frac{1}{2 \cdot \pi \cdot k_s} \cdot \ln\left(\frac{d_{ext}}{d_{int}}\right) + \frac{1}{h_c \cdot \pi \cdot d_{int}}} \tag{18}$$

Where Re_D is the Reynolds number calculated in the system, in Eq. (18) the dimensionless parameters *E*, *F*, *H*, F_{rh} and W_{el} were taken from a study by Pye (2008). The k_s is the average thermal conductivity of the pipe according to the specified material and d_{int} is the inner diameter of the tube.

Using the Dittus-Boelter correlation, the convective heat transfer coefficient of the working fluid, h_c, in both phases in Eqs. (19) and (20) was calculated, according to Odeh et al. (1998) this estimative yields better results for long and straight tubes as is the LFR system.

$$h_c = 0.023 \cdot Re_D^{0.8} \cdot Pr^{0.4} \cdot \frac{k}{d_{int}} \tag{19}$$

$$h_c = 0.023\left(\frac{\frac{\dot{m}}{A}(1-x)d_{int}}{\mu_l}\right)^{0.8} \cdot Pr^{0.4} \cdot \frac{k}{d_{int}} \tag{20}$$

Where *Pr* is the Prandtl number, *k* is the thermal conductivity of the working fluid at the saturation temperature and μ_l is the dynamic viscosity of the fluid at the saturation temperature.

The set of equations described above was solved using the Maple software and the thermal properties of the working fluid were collected through the EES software. Simulations with different DNI values were made to compare their effects on the system.

3. RESULTS AND DISCUSSIONS

To initiate the simulation was necessary to seek the value of the thermal conductivity and stiffness of the pipe, all coming from Sahoo et al. (2012a). It was also necessary to obtain the thermal and geometric properties of the reflective mirrors field, such as reflected area, transmissivity and reflectance of the mirrors, the latter two being taken from the study by Sahoo et al. (2012a).

Simulations were performed with 3 different DNI values, *700, 800 and 900* W/m^2, all considering an initial pressure of the fluid of 20 bar when entering the absorption tube, which also defined the saturation temperature of the working fluid at *212.4 ° C*, and consequently the exit temperature since in that study did not considered that the steam delivered to the power cycle would be in superheated state. For all simulations the average temperature of *28 ° C* in the city of Natal / RN was considered as the ambient temperature and as the initial temperature of the working fluid, while the initial temperature in the external wall of the tube of *32.4 ° C*, but due to the flow of heat directly focusing into the tubes, this value increases along the length of the tube. The mass flow in each tube was $0.115 kg/s$.

In Figure (5), the behavior of working fluid temperature is shown. For each DNI value, the saturation temperature was reached in different lengths, and with the highest DNI, the biphasic region was reached faster. The saturation temperatures were reached in *156*, *133* and *116* meters, respectively in the DNI's of *700, 800 and 900* W/m^2.

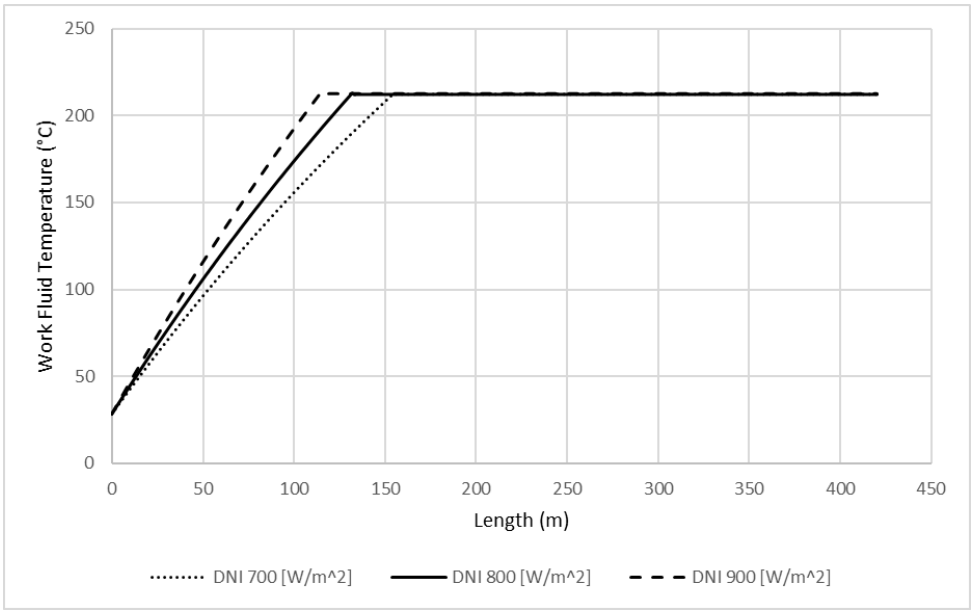

Figure 5. Graph Temperature x Length

In Figure (6) is shown the title, in other words, the parameter that indicates the quality of the steam that will be delivered to the power generation cycle. It was observed that higher the DNI in an LFR system, greater the percentage of dry steam produced and, consequently, better the quality of steam delivered to the cycle. This statement corroborates with the results of the working fluid temperature, because with the increase of DNI, the single-phase region will be smaller, with a longer pipe length for the biphasic region increasing the steam quality.

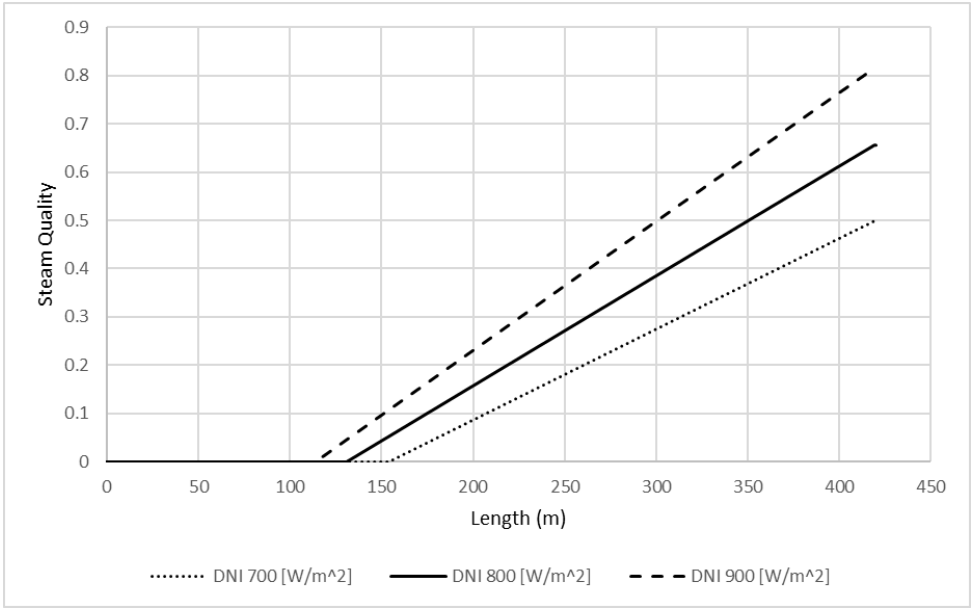

Figure 6. Graph steam quality x Length

The Figure (7) shows the pressure drop throughout the LFR system, in which case the increase of DNI in the system causes a greater pressure drop along the tube. This is justified by the fact that in the single-phase region, the pressure drop is caused mainly by the friction between the fluid and the tube, whereas in the biphasic region, the pressure drop depends on the friction and steam quality. Is easy observe that in the single-phase region the pressure drop is linear, contrasting with the pressure drop in the biphasic region, due to the correlations used in the biphasic region. Therefore, the pressure drop is accentuated in the biphasic region, especially after the steam quality exceeds *0.3*, and as the length of this region increases concomitantly with the DNI increase, this higher-pressure drop in high DNI values was already expected.

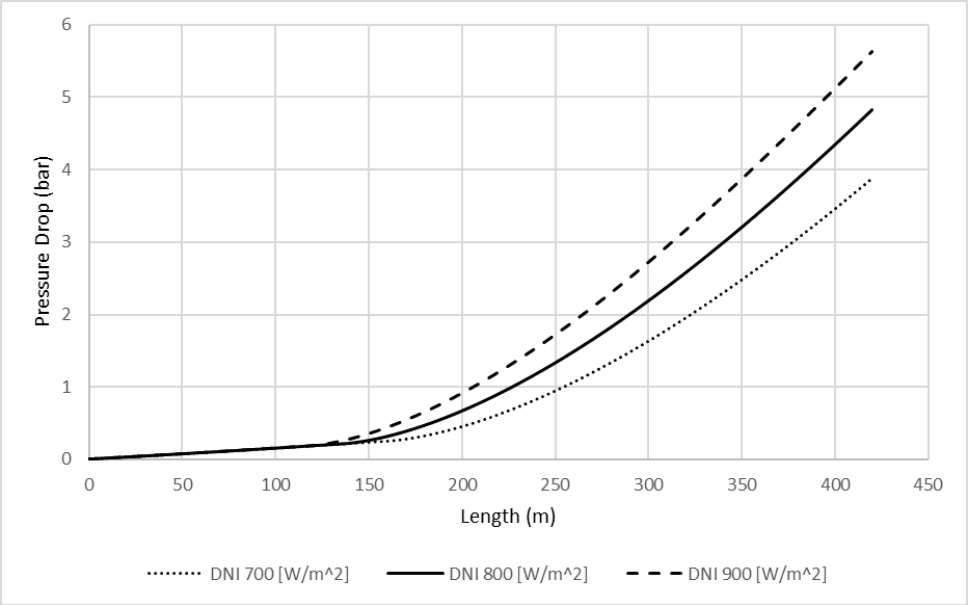

Figure 7. Graph pressure drop x Length

4. CONCLUSIONS

To understand the operation of an LFR system a thermo-hydraulic analysis in the absorption tubes was done through simulations. After studying both regions, biphasic and single-phase, and taking into account the results obtained in the simulations, it became evident how important the DNI is for the performance of the LFR system. That variation considerably modifies important parameters like pressure drop and steam quality that will be delivered to the power cycle.

The using viability of the LFR system to generate electricity for industries is recommended by the following reasons:

- The area occupied by solar fields is low compared to other CSP systems;
- Use of thin and flat mirrors that have a low cost and easy maintenance;
- Operates easily with direct steam generation;

Therefore, countries that are not recognized for being technological powerhouses but have areas for free use and are benefited by high DNI values can use Fresnel technology and obtain good returns for electric power generation or industrial processes.

The model obtained satisfactory results in the simulations, reaching a good quality of steam delivered to the power generation cycle. The pressure drop had a difference of the results obtained by Singh (2010) and Sahoo (2012a), but the used configurations were different, for example, pipe length and initial working fluid pressure, which are parameters directly connected to the thermo-hydraulic analysis of the system. For future research, is recommended for some considerations to be implemented to bring the simulation closer to reality. Such as:

- Estimate the overall heat loss coefficient instead of using an average value, leaving the calculations with a smaller margin of error;
- Use DNI values obtained by a transient analysis;
- Perform the efficiency calculation by adding the optical loss considerations of the LFR system;
- Minimize heat loss in the absorber cavity in order to optimize the system and produce more power.
- Perform analysis with other work fluids and different mass flows to see which will achieve the best results.

5. ACKNOWLEDGEMENTS

The team of Thermal Systems and Alternative Energies Laboratory of Federal University of Rio Grande do Norte supported this paper.

6. REFERENCES

AREVA (France). “Areva Solar Applications”. 15 Jan. 2017 <http://www.new.areva.com/EN/solar-232/arevasolarapplications.html>.

Balaji C, Venkatesan S. Correlations for free convection and surface radiation in square cavity. Int J Heat Fluid Flow 1994; 15(3):249–51.

Carnahan, B., Luther, H.A., Wilkes, J.O., 1969. q. New York: Wiley.

Cau, G. and Cocco, D., 2014. "Comparison of medium-size concentrating solar power plants based on parabolic through and linear Fresnel collectors". *In Proceedings of the 68th Conference of the Italian Thermal Machines Engineering Association*, ATI 2013.

Morin, G., Karl, M., Mertins, M., Selig, M. 2015. "Molten Salt as a heat transfer fluid in a linear Fresnel collector-commercial application backed by demonstration". *International Conference on Concentrating Solar Power and Chemical Energy Systems, SolarPACES 2014.*

Odeh, S.D., Morrison, G.L., Behnia, M., 1998. "Modelling of parabolic through direct steam generation solar collectors". *Solar Energy 62*, 395–406.

Pye, J.D., 2008. "System modeling of compact linear Fresnel reflector". Ph.D. Thesis. University of New South Wales, Australia.

Sahoo, S.S., Singh, S. and Banerjee, R. 2012a. Steady state hydrothermal analysis of the absorber tubes used in Linear Fresnel Reflector solar thermal system. Department of Mechanical Engineering, College of Engineering and Technology, Biju Patnaik University of Technology, Bhubaneswar, India.

Sahoo, S.S., Singh, S., Banerjee, R., 2012b. Analysis of heat losses from a trapezoidal cavity used for a linear Fresnel reflector system. *Solar Energy 86*, 1313–1322.

Silva Junior, J. L., 2015. "Análise térmica de um concentrador solar Fresnel". Trabalho de Conclusão de Curso. Universidade Federal do Rio Grande do Norte, Brasil.

Singh, P.L., Sarviya, R.M. and Bhagoria, J.L. 2010. Heat loss study of trapezoidal cavity absorbers for linear solar concentrating collector.

Swamee, P.K., Jain, A.K., 1976. "Explicit equations for pipe-flow problems". *Journal the Hydraulics Division (ASCE) 102*, 657–664.

Zhu, G., Wendelin, T., Wagner, M.J. and Kustler, C. 2013. History, current state, and future of linear Fresnel concentrating solar collectors.

7. RESPONSIBILITY NOTICE

The authors are the only responsible for the printed material included in this paper.